Exterior Clock-Integrity Auditing via Canonical Coherence of the Schumann Resonance Field

Kyle W. Luecke
Driftbound Labs · ORCID: 0009-0008-0202-7852 · admin@driftboundlabs.com
Version 2.0 — November 2026 (Supersedes August 2026 manuscript_v11.pdf)
Artifact & Provenance Repository: https://github.com/k-luecke/time-integrity

---

Abstract

Two-way packet time synchronization (NTP, IEEE 1588 PTP) has a fundamental algebraic blind spot: two directional timestamps cannot simultaneously solve for three unknowns (clock offset, forward path delay, and reverse path delay). An adversary who introduces asymmetric buffering on the physical link shifts the receiver's inferred clock without altering the round-trip time or violating cryptographic packet authentication. Detecting such an attack requires an exterior physical timing signal shared across the baseline. We evaluate the global Schumann resonance magnetic field (6–25 Hz) as an exterior reference across the 3 002 km LIGO Hanford–Livingston (H1–L1) baseline. Because horizontal magnetic waves arrive with unknown elliptical polarization and arbitrary sensor orientation, single-axis coherence severely underestimates inter-site coupling. We instead use **canonical coherence**—the maximum coherence achievable over any linear combination of the two horizontal sensor axes at each site—which is automatically invariant to compass rotation, gain mismatch, and cross-axis mixing. In a preregistered 6-hour O3 matched-vault run (`2020-01-29 01:53:02–07:53:02 UTC`), fundamental-mode canonical coherence reaches $\gamma^2_{\text{can}}(f_1) = 0.3291$ ($z = 24.54$ above the off-band empirical null $\mu_0 = 0.0399 \pm 0.0118$), a $49.9\times$ like-for-like gain over an unshielded GW170814 pilot ($\gamma^2_{\text{O3,corr}} = 0.2892$ vs. $\gamma^2_{\text{pilot,corr}} = 0.0058$), passing both block-permutation ($p < 0.048$) and phase-randomization null tests. Translating this coherence spectrum into Carter's Cramér–Rao lower bound yields a measured 6-hour timing precision floor of $\sigma_\tau = 76.6\,\mu$s ($45.7\,\mu$s raw). In contrast, direct time-domain lag extraction across twelve 30-minute windows recovers a physically bounded median lag of -3.85 ms ($11/12$ windows significant at $p \leq 0.05$) but fails the preregistered inter-window stability gate (`D2b`), exhibiting a 4.95 ms robust scatter (MADN) driven by diurnal lightning-storm migration. These results establish a sub-$100\,\mu$s physical information bound across a continental baseline and identify geophysical source-phase wander as the key bottleneck between the theoretical bound and operational clock auditing.

---

1. The Two-Way Timing Blind Spot and Exterior Reference Selection

In any two-way packet timing protocol between sites A and B (Mills et al. 2010; IEEE Standard for a Precision Clock Synchronization Protocol for Networked Measurement and Control Systems 2020), exchanging timestamps measures two directional time differences:

$$\Delta t_{\text{fwd}} = \theta + d_{\text{fwd}}, \qquad \Delta t_{\text{rev}} = -\theta + d_{\text{rev}},$$

where θ is the true clock offset between the sites, and $d_{\text{fwd}}, d_{\text{rev}} > 0$ are the one-way travel times. Subtracting the two measurements yields

$$\underbrace{\frac{\Delta t_{\text{fwd}} - \Delta t_{\text{rev}}}{2}}_{\text{protocol estimate } \hat{\theta}} = \underbrace{\theta}_{\text{true clock offset}} + \underbrace{\frac{d_{\text{fwd}} - d_{\text{rev}}}{2}}_{\text{hidden path asymmetry } (\Delta d/2)}.$$

Because two equations cannot solve for three unknowns $(\theta, d_{\text{fwd}}, d_{\text{rev}})$, every two-way protocol must assume symmetric travel times ($\Delta d \equiv d_{\text{fwd}} - d_{\text{rev}} = 0$) (Mizrahi 2014; Narula and Humphreys 2018). An on-path attacker who delays forward packets by $+\delta$ and advances reverse packets by $-\delta$ shifts the estimated clock by

$\widehat{\theta} - \theta = \delta/2$ while leaving the round-trip delay $d_{\text{fwd}} + d_{\text{rev}}$ unchanged. Cryptographic authentication (NTS (Franke et al. 2020), PTPsec) protects timestamp payloads from tampering but cannot detect physical packet buffering, and multi-path routing merely shifts the symmetry assumption to a majority of links (Mizrahi 2014).

Breaking this degeneracy requires an independent, out-of-band physical observable governed by four criteria:

1. **R1 (Global Reach):** Coherent visibility across continental baselines ($> 10^3$ km) without line-of-sight repeaters.
2. **R2 (Propagation Stability):** Phase velocity near c with millisecond-scale group delay across continental distances.
3. **R3 (Spoofing Hardness):** Natural excitation power far exceeding localized anthropogenic transmitters.
4. **R4 (Continuous Excitation):** Persistent natural drive requiring no cooperative beacon infrastructure.

Global lightning activity ($\sim$ 50–100 flashes/s, $\sim 10^{11}$ W aggregate electromagnetic power) continuously rings the Earth–ionosphere cavity at its electromagnetic eigenfrequencies—the Schumann resonances ($f_1 \approx 7.8$ Hz, $f_2 \approx 14.1$ Hz, $f_3 \approx 20.3$ Hz, $f_4 \approx 26.4$ Hz) (Schumann 1952; Nickolaenko and Hayakawa 2002). Propagating in the extremely low frequency (ELF) band (6–25 Hz) with minimal attenuation ($\sim$ 0.2–0.5 dB/Mm), the Schumann magnetic field satisfies **R1–R4** while penetrating deep underground vaults that block GNSS and radio signals (Thrane et al. 2013; Coughlin et al. 2018).

---

2. Canonical Coherence and the Carter Timing Bound

2.1 Why Single-Axis Coherence Fails—and How Canonical Coherence Fixes It

At two distant sites H (Hanford) and L (Livingston), horizontal two-axis magnetometers record vector time series $\mathbf{x}_H(t) = [x_{HX}(t), x_{HY}(t)]^\top$ and $\mathbf{x}_L(t) = [x_{LX}(t), x_{LY}(t)]^\top$. For any single axis $i \in \{X, Y\}$ at Hanford and $j \in \{X, Y\}$ at Livingston, ordinary scalar magnitude-squared coherence measures the fraction of shared power at frequency f (Welch 1967; Thomson 1982):

$$\gamma^2_{ij}(f) = \frac{|S_{H_iL_j}(f)|^2}{S_{H_iH_i}(f)\, S_{L_jL_j}(f)} \in [0, 1],$$

where $S_{H_iL_j}(f)$ is the cross-spectral density and $S_{H_iH_i}(f), S_{L_jL_j}(f)$ are the auto-spectral densities.

In a spherical waveguide, however, horizontal magnetic waves are elliptically polarized and arrive at different azimuths at different sites (Nickolaenko and Hayakawa 2002). If a wave arrives at 45° to the sensor axes, or if the two sites have different compass orientations, energy is split across the X and Y channels and every single-pair coherence $\gamma^2_{ij}(f)$ looks artificially small.

Instead of picking a single axis pair, **canonical coherence** (Koopmans 1974; Brillinger 1981) asks: *What is the maximum coherence achievable if we form an optimal virtual antenna* $\mathbf{u} \in \mathbb{C}^2$ *at Hanford and* $\mathbf{v} \in \mathbb{C}^2$ *at Livingston?*

$$\lambda_1(f) = \max_{\mathbf{u},\mathbf{v} \neq \mathbf{o}} \frac{|\mathbf{u}^\dagger \mathbf{S}_{HL}(f)\mathbf{v}|^2}{(\mathbf{u}^\dagger \mathbf{S}_{HH}(f)\mathbf{u})(\mathbf{v}^\dagger \mathbf{S}_{LL}(f)\mathbf{v})} \in [0, 1],$$

where $\mathbf{S}_{HH}(f)$ and $\mathbf{S}_{LL}(f)$ are the 2×2 site auto-spectral matrices and $\mathbf{S}_{HL}(f)$ is the 2×2 cross-spectral matrix. By standard linear algebra, this maximum is the largest eigenvalue $\lambda_1(f)$ of $\mathbf{C}(f)\mathbf{C}^\dagger(f)$ (equivalently of $\mathbf{S}^{-1}_{HH}(f)\mathbf{S}_{HL}(f)\mathbf{S}^{-1}_{LL}(f)\mathbf{S}_{LH}(f)$, followed by a second orthogonal eigenvalue $\lambda_2(f)$), where

$$\mathbf{C}(f) = \mathbf{S}^{-1/2}_{HH}(f)\, \mathbf{S}_{HL}(f)\, \mathbf{S}^{-1/2}_{LL}(f)$$

is the whitened cross-spectral matrix. We define our primary fundamental-mode statistic $\gamma^2_{\text{can}}(f_1)$ as the average of $\lambda_1(f)$ across the fundamental Schumann band $[7.3, 8.3]$ Hz.

Automatic Calibration Invariance: Suppose the sensor axes at either site are rotated, miscalibrated in gain, or cross-coupled by any invertible 2×2 matrix ($\mathbf{x}_H \mapsto \mathbf{A}_H \mathbf{x}_H$ and $\mathbf{x}_L \mapsto \mathbf{A}_L \mathbf{x}_L$). In the maximization above, this simply re-labels the weight vectors ($\mathbf{u} \mapsto \mathbf{A}_H^{-\dagger}\mathbf{u}$, $\mathbf{v} \mapsto \mathbf{A}_L^{-\dagger}\mathbf{v}$), leaving the maximum $\lambda_1(f)$ completely unchanged (Brillinger 1981). Canonical coherence therefore recovers the full shared wavefield without compass alignment or gain calibration.

2.2 From Canonical Coherence to Carter's Timing Bound

In spectral estimation theory, each canonical coherence $\lambda_1(f)$ represents the fraction of variance in the dominant eigenchannel at frequency f shared between the two sites, while $1-\lambda_1(f)$ is the unshared noise fraction. Their ratio defines the **effective coherent signal-to-noise ratio** at frequency f (Carter 1987):

$$\text{SNR}_{\text{eff}}(f) = \frac{g(f)}{1 - g(f)}, \qquad g(f) \equiv \max(\lambda_1(f) - \mu_0,\, 0),$$

where subtracting the empirical off-band null mean μ_0 (computed across inter-mode off-band windows) prevents finite-sample eigenvalue bias from inflating the SNR, and bounds are evaluated for both raw ($g = \lambda_1$) and bias-corrected spectra.

If the clock at site L shifts by a time offset τ relative to site H, the cross-spectrum at frequency f rotates in phase by $\Delta\phi(f) = 2\pi f \tau$. Carter's Cramér–Rao lower bound (CRLB) (Knapp and Carter 1976; Carter 1987) states that the minimum possible timing uncertainty $\sigma_\tau(T)$ of any unbiased delay estimator over integration time T is governed by three physical factors:

$$\sigma_\tau(T) \geq \left[\underbrace{2T}_{\substack{\text{integration} \\ \text{time}}} \int_{f_{\text{min}}}^{f_{\text{max}}} \underbrace{(2\pi f)^2}_{\substack{\text{phase-slope} \\ \text{leverage}}} \underbrace{\frac{g(f)}{1 - g(f)}}_{\text{SNR}_{\text{eff}}(f)} \, df \right]^{-1/2}.$$

Reading each term under the square root shows how coherence sets the timing floor:

1. **Integration time ($2T$):** Longer observation windows average down random phase fluctuations as $\sigma_\tau \propto T^{-1/2}$ under stationary coupling.
2. **Phase-slope leverage ($(2\pi f)^2$):** Higher frequencies produce a steeper phase shift per microsecond of delay, weighting coherent upper Schumann bands heavily.
3. **Coherent SNR ($g/(1-g)$):** As null-corrected canonical coherence $g(f_1)$ rises from 0.0058 (unshielded pilot) to 0.2892 (shielded vault), the effective SNR inside the integral jumps by nearly two orders of magnitude, shrinking $\sigma_\tau(T)$ by nearly an order of magnitude.

Detecting a Clock-Drift Ramp (Proposition 1): If an attacker injects a gradual clock-drift ramp $\theta(t) = \dot{\theta} t$ rather than a static step, the offset grows linearly with time. Integrating the squared drift signal $(\dot{\theta} t)^2$ against white estimation noise $\sigma_\tau^2(T_0)$ over duration T accumulates detection SNR as $\text{SNR}^2_{\text{ramp}}(T) \propto \dot{\theta}^2 T^3 / \sigma_\tau^2(T_0)$. Solving for the time required to reach a fixed detection threshold yields the cube-root scaling

$$T_{\text{det}} \propto \left(\frac{\sigma_\tau(T_0)}{\dot{\theta}} \right)^{2/3},$$

subject to a minimum spectral-window floor ($T_{\text{min}} \gtrsim 32$–$96$ s for multi-segment 16 s Welch averaging) and $1/f$ flicker or geophysical phase wander at multi-hour horizons.

---

3. Empirical Evaluation Across the LIGO H1–L1 Baseline

3.1 Datasets and Preregistered Pipeline

We test the method across the $3\,002$ km baseline between LIGO Hanford (H1, Washington) and LIGO Livingston (L1, Louisiana)—where vacuum light-travel time is 10.0 ms and Earth–ionosphere waveguide delay is ≤ 15 ms (≈ 13.0 ms at $v_{\text{ph}} \approx 0.77c$)—using public auxiliary magnetometer channels (Nguyen et al. 2021) from the Gravitational Wave Open Science Center (GWOSC) (Abbott et al. 2023):

1. **GW170814 Pilot (Asymmetric Shielding, $T = 2.63$ h):** Two quiet epochs near GW170814 pairing an unshielded H1 corner-station fluxgate (`H1:PEM-CS_MAG_LVEA_VERTEX_X/Y_DQ`, exposed to 60 Hz building power and electronics) with a shielded L1 vault induction magnetometer (`L1:PEM-EY_VAULT_MAG_LEMI_X/Y_DQ`).
2. **Preregistered O3 Matched-Vault Run ($T = 6.00$ h):** A continuous 6-hour quiet epoch (`2020-01-29 01:53:02–07:53:02 UTC`, GPS `1264298000–1264319600`) pairing the isolated H1 subterranean vault coil (`H1:PEM-VAULT_MAG_1030X195Y_COIL_X/Y_DQ`) with the L1 subterranean vault LEMI (`L1:PEM-EY_VAULT_MAG_LEMI_X/Y_DQ`) (Coughlin et al. 2018; Nguyen et al. 2021).

All channels are decimated from $4\,096$ Hz to 128 Hz ($2\,764\,800$ samples/channel) and analyzed using Welch's method (Welch 1967) with 16 s Hann windows ($2\,048$ samples, $\Delta f = 1/16$ Hz $= 0.0625$ Hz) and 50% overlap ($1\,024$ samples, $N_{\text{avg}} = 2\,699$ segments over 6 h). Surrogate block permutations use 64 s vector blocks so block boundaries greatly exceed the 16 s spectral window. All pass/fail gates (`G0`, `P1`, `P2`, `N1/N2`, `D1`, `D2a`, `D2b`) were frozen before running on O3 data in the open provenance package `k-luecke/time-integrity` (frozen protocol `preregistration/o3_vault_run.py`, SHA-256 `f45dca61…`; executed serialization fix `analysis/o3_vault_run_v4_1.py`, SHA-256 `98a27d1b…`, differing by exactly two post-verdict archive bytes) (Luecke 2026).

3.2 Spectral and Surrogate-Null Results

In the GW170814 pilot, local building noise at the unshielded H1 sensor held raw canonical coherence to $\gamma^2_{\text{can,raw}}(f_1) = 0.0103$ and off-band-null-corrected canonical coherence to $\gamma^2_{\text{pilot,corr}}(f_1) = 0.0058$ ($z = 9.7$). Moving the H1 sensor to the isolated subterranean vault in O3 removes building interference and boosts like-for-like null-corrected canonical coherence by $49.9\times$ ($56.4\times$ relative to the N1 block-permutation mean).

Metric / Preregistered Gate	Criterion / Definition	O3 Result (`2020-01-29`, 6 h)	Verdict
G0: Data & Conditioning Gate	$\geq 90\%$ retrieval across 4 channels; well-conditioned $\mathbf{S}_{HH}, \mathbf{S}_{LL}$	100.0% retrieval (0% dropout); condition number median 1.5, max 1.8	**Supported** (`PASS`)
Single-Axis Pairs at f_1	$\gamma^2_{ij}(f_1)$ averaged over $[7.3, 8.3]$ Hz	$H_X L_X = 0.0215$, $H_X L_Y = 0.1477$, $H_Y L_X = 0.1584$, $H_Y L_Y = 0.0974$	Cross-axis dominant
P1: Physical Coherence at f_1	$z(f_1) \geq 5$ over off-band null $\mu_0 \pm \sigma_0$, plus N1 & N2 collapse	$\gamma^2_{\text{can}}(f_1) = 0.3291$ vs. $\mu_0 = 0.0399 \pm 0.0118$ ($z = 24.54$)	**Supported** (`PASS`)
P2: Sensor Shielding Prediction	$\gamma^2_{\text{can,raw}}(f_1) \geq 0.10$; secondary $R = \gamma^2_{\text{O3,corr}}/0.0058 \in [30, 100]$	$0.3291 \geq 0.10$; $R = 0.2892/0.0058 = 49.9\times$ ($56.4\times$ vs. N1 mean)	**Supported** (`UPHELD`)
N1: Block-Permutation Null	20 random permutations of L1 64 s two-axis vector blocks	Mean $= 0.0020$, Max $= 0.0065$ ($p < 1/21 = 0.0476$)	**Supported** (`PASS`)
N2: Phase-Randomization Null	Random Fourier phases applied to L1 channels ($+60$ s shift secondary)	$\gamma^2_{\text{can,N2}}(f_1) = 0.0014$; $+60$ s shift $= 0.0018$	**Supported** (`PASS`)

Metric / Preregistered Gate	Criterion / Definition	O3 Result (`2020-01-29`, 6 h)	Verdict
D1: Carter Timing Bound (6 h)	$\sigma_\tau(6\,\mathrm{h}) < 1$ ms across 6–25 Hz (raw & null-subtracted agree)	$45.7\,\mu$s (raw) / $76.6\,\mu$s (off-band null-subtracted)	**Supported** (`PASS`)
D2b: 30-min Lag Stability	$> 6/12$ windows $p \le 0.05$, $\lvert\tau_{\mathrm{med}}\rvert \le 15$ ms, MADN ≤ 0.796 ms	$11/12$ windows $p \le 0.05$; $\tau_{\mathrm{med}} = -3.85$ ms; MADN $= 4.95$ ms	**Not supported** (`NOT PASSED` — lag stability failed)

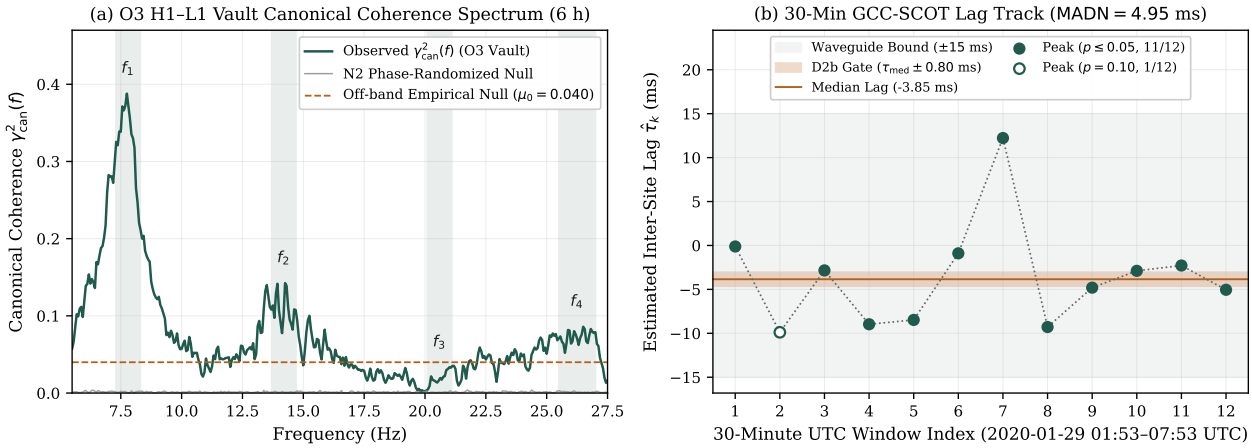


Figure 1: Observed O3 H1–L1 subterranean vault canonical coherence spectrum and 30-minute physical lag track across the 6-hour coincident interval (`2020-01-29 01:53:02–07:53:02 UTC`, GPS `1264298000–1264319600`). **(a)** Canonical coherence $\gamma^2_{\mathrm{can}}(f)$ peaks sharply on the fundamental ($f_1 = 0.3291$) and second ($f_2 = 0.1083$) Schumann modes above the empirical off-band baseline ($\mu_0 = 0.0399$) and N2 phase-randomized surrogate (0.0014). **(b)** Four-pair orientation-free GCC-SCOT lag estimates across twelve 30-minute windows yield $11/12$ significant detections ($p \le 0.05$) and a physically bounded median ($\tau_{\mathrm{med}} = -3.85$ ms), but wander by MADN $= 4.95$ ms across $[-9.89, +12.23]$ ms, exceeding the stationary D2b stability band (± 0.80 ms).

Two physical signatures confirm that the observed coupling is genuine global Schumann resonance wavefield structure rather than narrowband instrumental lines:

1. **Why Canonical Coherence Doubles Single-Axis Coherence:** Parallel-axis coherences ($H_X L_X = 0.0215$, $H_Y L_Y = 0.0974$) are weak because the wavefield is cross-polarized between sites ($H_X L_Y = 0.1477$, $H_Y L_X = 0.1584$). Canonical coherence ($\gamma^2_{\mathrm{can}}(f_1) = 0.3291$) automatically combines both horizontal axes at each vault to capture the full elliptically polarized mode, exceeding the best single-axis pair by $2.08\times$.
2. **Modal Resonance Structure:** As shown in Figure 1(a), canonical coherence peaks on the lower Schumann eigenmodes—$\gamma^2_{\mathrm{can}}(f_1) = 0.3291$ (7.3–8.3 Hz) and $\gamma^2_{\mathrm{can}}(f_2) = 0.1083$ (13.7–14.7 Hz)—rising cleanly above the adjacent inter-mode troughs (0.0435 in 10.5–12.5 Hz and 0.0291 in 16.5–18.5 Hz). Coupling attenuates at $f_3 = 0.0200$ (20.1–21.1 Hz), consistent with nodal baseline geometry at $\sim$ 3 Mm separation (Nickolaenko and Hayakawa 2002), before showing modest recovery near $f_4 = 0.0726$ (25.5–27.0 Hz).

---

4. Information Bound (`D1`) vs. Physical Lag Wander (`D2b`)

Integrating the off-band-null-subtracted O3 canonical coherence across 6–25 Hz in Carter's bound (**D1**) yields a measured 6-hour timing precision floor of $\sigma_\tau = 76.6\,\mu$s ($45.7\,\mu$s raw). Scaled to a single 30-minute window, the theoretical floor is $\sigma_{\tau,30\mathrm{m}} = 76.6\,\mu\mathrm{s} \times \sqrt{12} = 265\,\mu$s, which sets the preregistered 3σ inter-window

stability threshold $\max(3\sigma_{\tau,30\mathrm{m}}, 0.3\,\mathrm{ms}) = 0.796\,\mathrm{ms}$. Under a strict stationarity assumption on $\gamma^2_{\mathrm{can}}(f,t)$, longer integration **projects** (not measured here) to $38.3\,\mu$s ($22.8\,\mu$s raw) over 24 h and $6.99\,\mu$s ($4.17\,\mu$s raw) over 30 days.

To test whether an unmodeled time-domain cross-correlator can reach the $265\,\mu$s per-window floor without accounting for lightning source geometry, Gate **D2b** splits the 6-hour run into twelve 30-minute windows and evaluates a two-step orientation-free lag estimator across 6–25 Hz:

1. **Phase-Whitened Correlation (GCC-SCOT) per Axis Pair:** For each of the four horizontal axis pairs $(i,j) \in \{X,Y\}^2$, we normalize the cross-spectrum by the auto-spectral magnitudes (Smoothed Coherence Transform (Carter et al. 1973; Knapp and Carter 1976)) so that every frequency bin contributes whitened phase information, then transform back to time lag τ:

$$C_{ij}(\tau) = \mathcal{F}^{-1}\left\{ \frac{S_{H_iL_j}(f)}{\sqrt{S_{H_iH_i}(f)\,S_{L_jL_j}(f)}} \right\}(\tau).$$

2. **Orientation-Free Energy Sum:** We sum the squared correlations across all four pairs and locate the peak over the physical ± 150 ms search interval via parabolic interpolation:

$$Q(\tau) = C^2_{XX}(\tau) + C^2_{XY}(\tau) + C^2_{YX}(\tau) + C^2_{YY}(\tau), \qquad \hat{\tau} = \arg\max_{\tau \in [-150,+150]\,\mathrm{ms}} Q(\tau).$$

Across the twelve 30-minute windows (Figure 1b), $11/12$ exceed all 19 in-window block-permutation surrogates ($p \le 0.05$), and the median lag $\tau_{\mathrm{med}} = -3.85$ ms sits well inside the ± 15 ms physical propagation limit between Hanford and Livingston. Nevertheless, **Gate D2b is not passed**: the window-to-window robust lag scatter is $\mathrm{MADN}(\hat{\tau}) = 4.95$ ms (with individual window peaks spanning -9.89 ms to $+12.23$ ms), exceeding the 0.796 ms stationary threshold by $6.2\times$ ($18.7\times$ the 0.265 ms per-window CRLB).

Why does the information bound allow $76.6\,\mu$s (**D1**) while raw time-domain peaks wander by 4.95 ms (**D2b**)?

- **What the Carter bound (`D1`) measures:** Carter's bound quantifies the intrinsic phase-reading precision *given a known or stationary propagation transfer function* between the two receivers (Carter 1987).
- **What changes in the real cavity (`D2b` — `PROPOSED` physical mechanism):** Global lightning is concentrated in three tropical continental "chimneys" (Maritime Continent/Asia, Africa, and the Americas) whose relative excitation migrates westward across the 6-hour UTC interval (Nickolaenko and Hayakawa 2002). Because the Schumann field is a partially standing spherical-waveguide interference pattern, shifting the dominant source region alters the wave arrival azimuth and rotates the inter-site cross-spectral phase $\arg \mathbf{S}_{HL}(f)$ by several milliseconds of apparent group delay—even while both LIGO observatories remain locked to GPS ($\theta_{HL} \approx 0$). In companion follow-on experiments archived at `k-luecke/Geo` using World Wide Lightning Location Network (WWLLN) stroke catalogs (Holzworth et al. 2019), neither contemporaneous 30-minute WWLLN energy maps (`wwlln_coherency_v12`) nor 128 Hz time-only stroke-to-transient association (`transient_commonview_v1`, $p_{\mathrm{emp}} = 0.4216$ against a 1,000-shift null) improved complex-coherency prediction or beat the null (**Not supported**), isolating full polarization/bearing plus waveguide transfer modeling as an open requirement.

---

5. Conclusion

1. **Closing the Two-Way Blind Spot:** The global Schumann resonance magnetic field (6–25 Hz) provides a continuous, vault-penetrating exterior physical timing channel that an on-path network adversary cannot buffer or spoof without overpowering global lightning excitation.
2. **Calibration-Free Signal Recovery:** Canonical coherence automatically combines two-axis horizontal magnetometers without compass or gain calibration, increasing null-corrected H1–L1 fundamental coherence $49.9\times$ (to $\gamma^2_{\mathrm{can}}(f_1) = 0.3291$, $z = 24.54$) when moving from unshielded facility sensors to subterranean vaults.

3. **The Source-Geometry Gap:** While the shared Schumann wavefield carries sufficient coherent phase information to bound continental clock offsets to $\sigma_\tau = 76.6\ \mu$s over 6 h (`D1`, **Supported**), unmodeled time-domain lag estimation fails inter-window stationarity (`D2b`, **Not supported**) with 4.95 ms scatter (`PROPOSED` cause: diurnal lightning-source migration). Reaching the sub-$100\ \mu$s Carter floor in operational exterior clock auditing—without claiming a standalone positioning system or GNSS replacement—requires forward-modeling or projecting out low-rank geophysical source-phase drift across a multi-station network.

Data Availability and Acknowledgments

All preregistered analysis code, SHA-256 provenance manifests, scored O3 outputs (`o3_results_v4_1_98a27d1b.json`), and derived cross-spectral states (`o3_spectra_v4_1_98a27d1b.npz`) are publicly archived under the Mozilla Public License 2.0 at https://github.com/k-luecke/time-integrity (Luecke 2026). Companion source-conditioned and transient common-view Schumann/WWLLN follow-on artifacts are archived at https://github.com/k-luecke/Geo.

The author gratefully thanks **Robert H. Holzworth** (University of Washington) and the **World Wide Lightning Location Network (`http://wwlln.net`)**, a collaboration among over 50 universities and institutions, for providing the WWLLN global lightning location data (Holzworth et al. 2019) used in the companion source-conditioned and transient common-view Schumann investigations (raw WWLLN stroke files are copyrighted by the University of Washington and are not redistributed).

This research has made use of data or software obtained from the Gravitational Wave Open Science Center (`gwosc.org`), a service of the LIGO Scientific Collaboration, the Virgo Collaboration, and KAGRA (Abbott et al. 2023). This material is based upon work supported by NSF's LIGO Laboratory which is a major facility fully funded by the National Science Foundation, as well as the Science and Technology Facilities Council (STFC) of the United Kingdom, the Max-Planck-Society (MPS), and the State of Niedersachsen/Germany for support of the construction of Advanced LIGO and construction and operation of the GEO600 detector. Additional support for Advanced LIGO was provided by the Australian Research Council. Virgo is funded, through the European Gravitational Observatory (EGO), by the French Centre National de la Recherche Scientifique (CNRS), the Italian Istituto Nazionale di Fisica Nucleare (INFN) and the Dutch Nikhef, with contributions by institutions from Belgium, Germany, Greece, Hungary, Ireland, Japan, Monaco, Poland, Portugal, Spain. KAGRA is supported by Ministry of Education, Culture, Sports, Science and Technology (MEXT), Japan Society for the Promotion of Science (JSPS) in Japan; National Research Foundation (NRF) and Ministry of Science and ICT (MSIT) in Korea; Academia Sinica (AS) and National Science and Technology Council (NSTC) in Taiwan.

References

Abbott, R., H. Abe, F. Acernese, et al. 2023. "Open Data from the Third Observing Run of LIGO, Virgo, KAGRA, and GEO." *The Astrophysical Journal Supplement Series* 267 (2): 29. https://doi.org/10.3847/1538-4365/acdc9f.

Brillinger, David R. 1981. *Time Series: Data Analysis and Theory*. Expanded. Holden-Day / SIAM. https://doi.org/10.1137/1.9780898719246.

Carter, G. Clifford. 1987. "Coherence and Time Delay Estimation." *Proceedings of the IEEE* 75 (2): 236–55. https://doi.org/10.1109/PROC.1987.13723.

Carter, G. Clifford, Albert H. Nuttall, and Peter G. Cable. 1973. "The Smoothed Coherence Transform." *Proceedings of the IEEE* 61 (10): 1497–98. https://doi.org/10.1109/PROC.1973.9300.

Coughlin, Michael W., Alessio Cirone, Patrick Meyers, et al. 2018. "Measurement and Subtraction of Schu-

mann Resonances at Gravitational-Wave Interferometers." *Physical Review D* 97 (10): 102007. https://doi.org/10.1103/PhysRevD.97.102007.

Franke, Daniel, Dieter Sibold, Kristof Teichel, Marcus Dansarie, and Ragnar Sundblad. 2020. *Network Time Security for the Network Time Protocol*. RFC No. 8915. Internet Engineering Task Force (IETF). https://doi.org/10.17487/RFC8915.

Holzworth, Robert H., Michael P. McCarthy, James B. Brundell, Abram R. Jacobson, and Craig J. Rodger. 2019. "Global Distribution of Superbolts." *Journal of Geophysical Research: Atmospheres* 124 (17–18): 9996–10005. https://doi.org/10.1029/2019JD030975.

IEEE Standard for a Precision Clock Synchronization Protocol for Networked Measurement and Control Systems, Pub. L. Nos. IEEE Std 1588-2019 (2020). https://doi.org/10.1109/IEEESTD.2020.9120376.

Knapp, Charles H., and G. Clifford Carter. 1976. "The Generalized Correlation Method for Estimation of Time Delay." *IEEE Transactions on Acoustics, Speech, and Signal Processing* 24 (4): 320–27. https://doi.org/10.1109/TASSP.1976.1162830.

Koopmans, Lambert H. 1974. *The Spectral Analysis of Time Series*. Academic Press.

Luecke, Kyle W. 2026. *Time Integrity: Preregistered O3 Both-Site Vault-Magnetometer Schumann Coherence and Lag Package*. Https://github.com/k-luecke/time-integrity.

Mills, David, Jim Martin, Jack Burbank, and William Kasch. 2010. *Network Time Protocol Version 4: Protocol and Algorithms Specification*. RFC No. 5905. Internet Engineering Task Force (IETF). https://doi.org/10.17487/RFC5905.

Mizrahi, Tal. 2014. *Security Requirements of Time Protocols in Packet Switched Networks*. RFC No. 7384. Internet Engineering Task Force (IETF). https://doi.org/10.17487/RFC7384.

Narula, Lakshay, and Todd E. Humphreys. 2018. "Requirements for Secure Clock Synchronization." *IEEE Journal of Selected Topics in Signal Processing* 12 (4): 749–62. https://doi.org/10.1109/JSTSP.2018.2835763.

Nguyen, P., R. M. S. Schofield, A. Effler, et al. 2021. "Environmental Noise in Advanced LIGO Detectors." *Classical and Quantum Gravity* 38 (14): 145001. https://doi.org/10.1088/1361-6382/ac011a.

Nickolaenko, Alexander P., and Masashi Hayakawa. 2002. *Resonances in the Earth–Ionosphere Cavity*. Kluwer Academic Publishers / Springer. https://doi.org/10.1007/978-94-010-0468-8.

Schumann, Winfried Otto. 1952. "Über Die Strahlungslosen Eigenschwingungen Einer Leitenden Kugel, Die von Einer Luftschicht Und Einer Ionosphärenhülle Umgeben Ist." *Zeitschrift für Naturforschung A* 7 (2): 149–54. https://doi.org/10.1515/zna-1952-0202.

Thomson, David J. 1982. "Spectrum Estimation and Harmonic Analysis." *Proceedings of the IEEE* 70 (9): 1055–96. https://doi.org/10.1109/PROC.1982.12433.

Thrane, Eric, Nelson Christensen, and Robert M. S. Schofield. 2013. "Correlated Magnetic Noise in Global Networks of Gravitational-Wave Detectors: Observations and Implications." *Physical Review D* 87 (12): 123009. https://doi.org/10.1103/PhysRevD.87.123009.

Welch, Peter D. 1967. "The Use of Fast Fourier Transform for the Estimation of Power Spectra: A Method Based on Time Averaging over Short, Modified Periodograms." *IEEE Transactions on Audio and Electroacoustics* 15 (2): 70–73. https://doi.org/10.1109/TAU.1967.1161901.